

# Scaling GraphLLM with Bilevel-Optimized Sparse Querying

Yangzhe Peng<sup>1</sup> Haiquan Qiu<sup>2</sup> Quanming Yao<sup>2</sup> Kun He<sup>1</sup>

## Abstract

LLMs have recently shown strong potential in enhancing node-level tasks on text-attributed graphs (TAGs) by providing explanation features. However, their practical use is severely limited by the high computational and monetary cost of repeated LLM queries. To illustrate, naively generating explanations for all nodes on a medium-sized benchmark like Photo (48k nodes) using a representative method (e.g., TAPE) would consume *days* of processing time. In this paper, we propose Bilevel-Optimized Sparse Querying (BOSQ), a general framework that selectively leverages LLM-derived explanation features to enhance performance on node-level tasks on TAGs. We design an adaptive sparse querying strategy that selectively decides when to invoke LLMs, avoiding redundant or low-gain queries and significantly reducing computation overhead. Extensive experiments on six real-world TAG datasets involving two types of node-level tasks demonstrate that BOSQ achieves orders of magnitude speedups over existing GraphLLM methods while consistently delivering on-par or superior performance. Our codes are available at: <https://anonymous.4open.science/r/Fast-Node-Explainer-7D3B>

## 1. Introduction

Recently, Large Language Models (LLMs) have demonstrated exceptional semantic comprehension and reasoning capabilities (Touvron et al., 2023), leading to significant interest in exploring their utility for Text-Attributed Graphs (TAGs), where nodes are characterized by rich textual information (Chen et al., 2024; Fang et al., 2025; Hu et al., 2020). However, the direct integration of LLMs and graphs remains challenging: while LLMs excel at sequential reason-

<sup>1</sup>School of Computer Science and Technology , Huazhong University of Science and Technology, Wuhan, China <sup>2</sup>Department of Electronic Engineering, Tsinghua University, Beijing, China. Correspondence to: Firstname1 Lastname1 <firstname.lastname1@xxx.edu>.

Preprint. February 11, 2026.

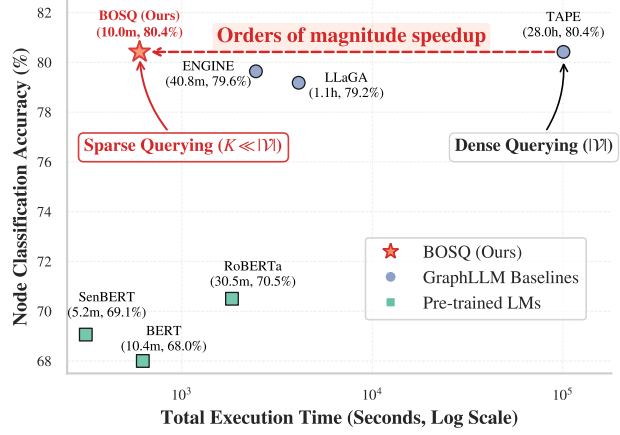


Figure 1. BOSQ significantly outperforms existing GraphLLM frameworks in efficiency without sacrificing task performance. By transitioning from Dense Querying to Sparse Querying via bilevel optimization, BOSQ reduces total end-to-end execution time by orders of magnitude compared to TAPE. Our method (red star) sits at the ideal top-left region, offering a practical and scalable solution for large-scale TAGs where traditional GraphLLM baselines are infeasible. Please refer to Table 2 for detailed results.

ing, they struggle to inherently capture the non-Euclidean structural dependencies and relational inductive biases that characterize graph-structured data.

To bridge this gap, recent studies have proposed integrating LLMs with graph learning methods, resulting in several emerging paradigms collectively referred to as GraphLLMs (Li et al., 2024). Specifically, three main approaches have been identified (Wu et al., 2025): 1. The **Encoder** paradigm utilizes LLMs to encode nodes' textual attributes, generating more expressive feature representations ( $h^{LLM}$ ) that surpass shallow embeddings, which are then aggregated by downstream GNNs (Zhu et al., 2024). 2. The **Predictor** paradigm involves LLMs directly serving as the classifier or regressor, consuming a structured prompt ( $\mathcal{P}$ ) constructed from the node's text and its aggregated neighborhood context to make a final, text-based prediction (Chen et al., 2024; Tang et al., 2024). The process can be abstracted as:  $\text{Pred}_i = \text{LLM}(\mathcal{P}_i)$ . 3. The **Explainer** paradigm leverages LLMs' generative capability to enhance node attributes by generating a detailed, semantic-rich **explanation feature**  $e^{exp}$  (He et al., 2024). This feature is derived from the node's textual context, and is designed to

augment the node’s original information, thereby enriching the node features before being processed by GNNs. Our work is primarily inspired by the Explainer paradigm, which utilizes the superior semantic comprehension of LLMs to generate high-quality, contextual explanation features that significantly enhance performance on node-level tasks.

However, a critical bottleneck severely restricts the practicality of these LLM-enhanced approaches: the **prohibitive computational and monetary cost** of exhaustive LLM querying across all nodes in the graph. Currently, all methods require invoking the LLM for every single node and thus the total cost scales linearly with the number of nodes  $|\mathcal{V}|$ :

$$C_{\text{total}} \propto |\mathcal{V}| \times C_{\text{LLM}}$$

where  $C_{\text{LLM}}$  denotes the cost of a single LLM query. For graphs of realistic size, e.g., tens or hundreds of thousands of nodes, this translates into days or even weeks of processing time and significant financial expense, rendering the approach infeasible for practical deployment, especially on medium to large-scale benchmark datasets.

Moreover, the assumption that every node contributes equally to the downstream task contradicts the principle of information sparsity observed in both biological and artificial neural networks (Bengio, 2017; Gao et al., 2025). Just as human cognition allocates attention selectively (the “spotlight” metaphor) (Posner, 1980) and recent sparse LLM architectures (Lu et al., 2025; Yuan et al., 2025) dynamically route computation to a subset of relevant components, graph data inherently exhibits structural and semantic redundancy. This observation suggests that the “brute-force” approach of dense querying is not only inefficient but potentially suboptimal due to noise accumulation. Inspired by these mechanisms of selective attention, we propose **Bilevel-Optimized Sparse Querying (BOSQ)**, an efficient and general explanation-guided framework. The core of BOSQ is an **adaptive sparse querying strategy** that intelligently selects a small, fixed-size budget of  $K$  nodes ( $K \ll |\mathcal{V}|$ ) for LLM interaction as illustrated in Figure 2. This selection is guided by learnable scores assigned to each node, which are optimized directly by backpropagating gradients from the downstream task’s validation loss. This task-driven mechanism ensures that the limited query budget is allocated to nodes whose explanation features provide the highest utility for improving the model’s performance, striking an optimal balance between efficiency and effectiveness.

Our contributions are summarized as follows:

- We propose **BOSQ**, a novel framework that efficiently integrates LLM-derived explanation features to boost node-level task performance on TAGs.
- **BOSQ** employs an **adaptive sparse querying strategy** leveraging bilevel optimization to dynamically prioritize and select nodes for LLM explanation queries.

- We empirically demonstrate that BOSQ achieves orders of magnitude speedups on six real-world TAG datasets while consistently maintaining competitive or even superior predictive performance.

## 2. Method

In this section, we present the detailed methodology of Bilevel-Optimized Sparse Querying (BOSQ), a framework that efficiently incorporates Large Language Model (LLM)-derived explanation features to enhance node-level tasks on Text-Attributed Graphs (TAGs). The core idea lies in an adaptive sparse querying strategy that selects a subset of nodes for explanation generation to balance performance and computational cost.

### 2.1. Preliminary

**Text-attributed graphs.** Formally, a text-attributed graph (TAG) (Ma & Tang, 2021) can be represented as  $\mathcal{G} = (\mathcal{V}, A, \{s_n\}_{n \in \mathcal{V}})$ , where  $\mathcal{V}$  is a set of  $N$  nodes,  $A \in \mathbb{R}^{N \times N}$  is the adjacency matrix, and  $s_n \in \mathcal{D}^{L_n}$  is a sequential text associated with node  $n \in \mathcal{V}$ , with  $\mathcal{D}$  as the words or tokens dictionary, and  $L_n$  as the sequence length.

**Node level tasks.** Consider a graph  $\mathcal{G}$  with a set of nodes  $\mathcal{V}$ . The nodes are partitioned into a labeled set  $\mathcal{V}_l \subset \mathcal{V}$  and an unlabeled set  $\mathcal{V}_u$ . The general objective of both node classification (node clf) and node regression (node reg) is to train a graph-based neural network model, utilizing the structure of  $\mathcal{G}$  and the known values of  $\mathcal{V}_l$ , to predict the corresponding unknown values (which can be discrete class labels or continuous values) for the nodes in  $\mathcal{V}_u$ . While the fundamental goal is shared, the definition of the unlabeled set  $\mathcal{V}_u$  differs: for node classification,  $\mathcal{V}_u$  comprises all remaining nodes ( $\mathcal{V}_u = \mathcal{V} \setminus \mathcal{V}_l$ ), whereas for node regression,  $\mathcal{V}_u$  only represents a specified subset of nodes (e.g., a particular type of node in a heterogeneous graph) whose continuous value is targeted for prediction.

**LLM-as-Explainer Paradigm** Recently, TAPE (He et al., 2024) have demonstrated that instead of directly encoding  $X_v$  using a shallow Language Model (LM), invoking a Large Language Model (LLM) to generate explanatory features significantly boosts performance. Formally, for each node  $n$ , a Large Language Model (LLM), denoted as  $\mathcal{M}_{\text{LLM}}$  with parameters  $\theta_{\text{LLM}}$ , is queried to transform the raw text  $s_n$  into a more informative explanatory text  $e_n$ :

$$e_n = \mathcal{M}_{\text{LLM}}(s_n; \theta_{\text{LLM}}) \quad (1)$$

The original text  $s_n$  and the LLM-generated explanation  $e_n$  are synthesized into an enriched textual attribute  $s'_n = \mathcal{T}(s_n, e_n)$ .  $\mathcal{T}$  can be implemented as a simple concatenation (i.e.,  $s_n \parallel e_n$ ) or a complete replacement (i.e.,  $s'_n = e_n$  or  $s'_n = s_n$ ).

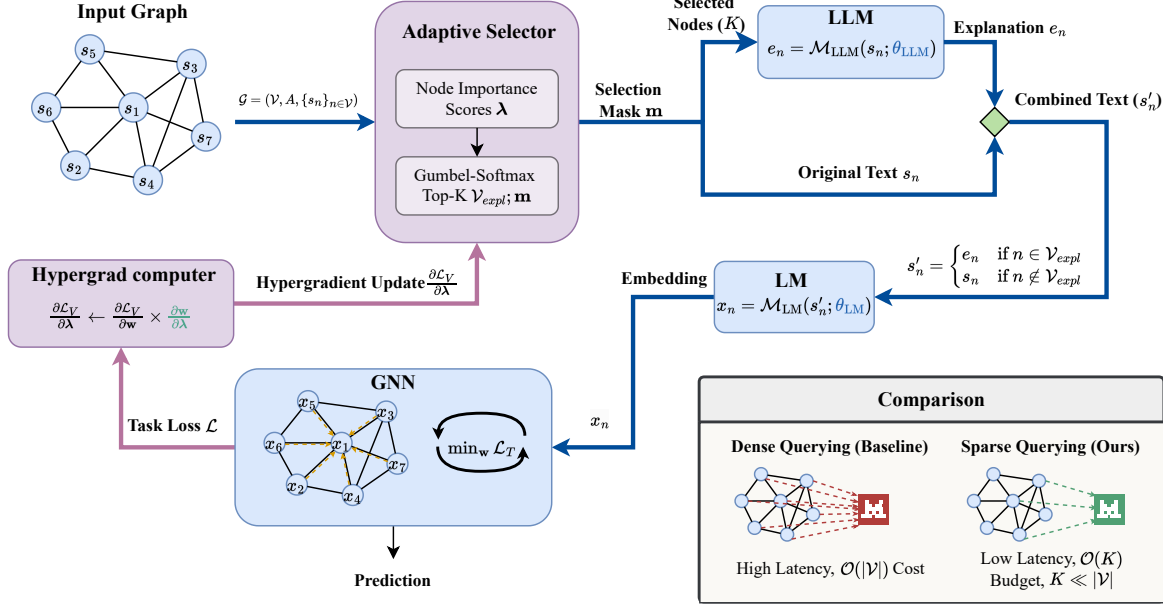


Figure 2. Overview of the BOSQ framework. Our method treats node selection as a bilevel optimization problem. The outer loop (purple) learns an Adaptive Selector to identify a sparse subset of nodes that benefit most from LLM explanations, while the inner loop (blue) optimizes a GNN on the resulting augmented graph. By using hypergradients to guide the selection mask  $\mathbf{m}$ , BOSQ selectively invokes the LLM only for critical nodes ( $K \ll |\mathcal{V}|$ ). This mechanism achieves a superior trade-off between task performance and computational efficiency compared to previous dense querying baselines (see Comparison box).

The integrated text  $s'_n$  is converted into a  $D$ -dimensional node embedding  $x_n$  using a Language Model (LM, e.g. RoBERTa),  $\mathcal{M}_{\text{LM}}$  with parameters  $\theta_{\text{LM}}$ :

$$x_n = \mathcal{M}_{\text{LM}}(s'_n; \theta_{\text{LM}}) \quad (2)$$

A Graph Neural Network (GNN),  $\mathcal{M}_{\text{GNN}}$  with parameters  $\mathbf{w}$ , takes as input the feature matrix  $X = [x_1, \dots, x_N]^T \in \mathbb{R}^{N \times D}$  and the adjacency matrix  $A$  to produce predictions  $\hat{Y}$ . The GNN is trained by minimizing the loss function  $\mathcal{L}$  over the training set  $\mathcal{V}_{\text{train}}$ . The prediction and optimization objectives are defined as follows:

$$\hat{Y} = \mathcal{M}_{\text{GNN}}(X, A; \mathbf{w}) \quad (3)$$

$$\min_{\mathbf{w}} \mathcal{L}_T(\hat{Y}, Y) = \min_{\mathbf{w}} \sum_{n \in \mathcal{V}_{\text{train}}} \ell(\hat{y}_n, y_n) \quad (4)$$

## 2.2. Bilevel-Optimized Sparse Querying

The core efficiency of our framework stems from the selective application of LLM explanations to a subset of nodes. To achieve this, we define a selection mask  $\mathbf{m} \in \{0, 1\}^N$ , where  $m_n = 1$  indicates that node  $n$  is selected for LLM explanation, and  $m_n = 0$  otherwise.

However, directly optimizing  $\mathbf{m}$  is a non-trivial combinatorial problem, which prevents the use of gradient-based optimization due to its discrete nature. While one could

rely on static heuristics (e.g., selecting nodes based on degree or entropy), such methods are task-agnostic and fail to capture the dynamic contribution of specific nodes to the downstream performance.

To bridge this gap, we propose to relax the discrete mask into a continuous importance vector  $\boldsymbol{\lambda} = (\lambda_1, \dots, \lambda_N)$ . By treating  $\boldsymbol{\lambda}$  as a differentiable proxy for the selection mask  $\mathbf{m}$ , we can formulate node selection as a bilevel optimization problem. In this setup, the outer loop optimizes the node importance scores  $\boldsymbol{\lambda}$  to maximize generalization on validation data, while the inner loop updates the model parameters  $\mathbf{w}$  based on the selected information. The transformation from continuous scores  $\boldsymbol{\lambda}$  to the final discrete mask  $\mathbf{m}$  is then performed through a top- $K$  sparsification process, which we detail in Section 2.3.

Formally, the bilevel optimization problem is formulated as:

$$\begin{aligned} \boldsymbol{\lambda}^* &:= \underset{\boldsymbol{\lambda}}{\operatorname{argmin}} \mathcal{L}_V^*(\boldsymbol{\lambda}) \quad \text{where} \\ \mathcal{L}_V^*(\boldsymbol{\lambda}) &:= \mathcal{L}_V(\boldsymbol{\lambda}, \mathbf{w}^*(\boldsymbol{\lambda})) \quad \text{and} \quad \mathbf{w}^*(\boldsymbol{\lambda}) := \underset{\mathbf{w}}{\operatorname{argmin}} \mathcal{L}_T(\boldsymbol{\lambda}, \mathbf{w}) \end{aligned} \quad (5)$$

where  $\mathcal{L}_{\text{train}}$  and  $\mathcal{L}_{\text{val}}$  denote the training and validation losses, respectively. By computing the hypergradient of the validation loss with respect to  $\lambda_n$ , we can accurately quantify each node's influence on the model's generalization ability, allowing the framework to prioritize explanations for the most “informative” nodes.

Equipped with the selection mask  $\mathbf{m}$  (derived from  $\boldsymbol{\lambda}$ ), we design a Sparse Querying architecture that selectively integrates LLM-derived features into the GNN pipeline. The forward pass proceeds through three core components:

$$s'_n = \begin{cases} \mathcal{M}_{\text{LLM}}(s_n; \theta_{\text{LLM}}) & \text{if } n \in \mathcal{V}_{\text{expl}} \\ s_n & \text{if } n \notin \mathcal{V}_{\text{expl}} \end{cases} \quad (6)$$

$$x_n = \mathcal{M}_{\text{LM}}(s'_n; \theta_{\text{LM}}) \quad (7)$$

$$\hat{Y} = \mathcal{M}_{\text{GNN}}(X, A; \mathbf{w}) \quad (8)$$

where  $\mathcal{V}_{\text{expl}} \subset \mathcal{V}$  represents the selected nodes to be explained. To ensure computational efficiency, we keep the parameters of the LLM ( $\theta_{\text{LLM}}$ ) and the LM ( $\theta_{\text{LM}}$ ) frozen, only optimizing the GNN parameters  $\mathbf{w}$ . The loss function  $\ell$  is instantiated as cross-entropy for node classification and  $L_1$  loss for node regression, following the standard practice in existing GraphLLM benchmarks (Robinson et al., 2024; Wu et al., 2025). Algorithm 1 illustrates the complete framework of our method.

### 2.3. Task-driven Optimization and Implementation

Having established the bilevel framework in equation 5, we now describe the task-driven optimization process for the importance scores  $\boldsymbol{\lambda}$  and the subsequent derivation of the selection mask  $\mathbf{m}$ . We optimize  $\boldsymbol{\lambda}$  by computing the hypergradient of the validation loss with respect to the node importance scores  $\frac{\partial \mathcal{L}_V^*(\boldsymbol{\lambda})}{\partial \boldsymbol{\lambda}}$ :

$$\frac{\partial \mathcal{L}_V^*(\boldsymbol{\lambda})}{\partial \boldsymbol{\lambda}} = \underbrace{\frac{\partial \mathcal{L}_V(\boldsymbol{\lambda}, \mathbf{w}^*(\boldsymbol{\lambda}))}{\partial \boldsymbol{\lambda}}}_{\text{direct grad.}} + \underbrace{\frac{\partial \mathcal{L}_V(\boldsymbol{\lambda}, \mathbf{w}^*(\boldsymbol{\lambda}))}{\partial \mathbf{w}^*(\boldsymbol{\lambda})} \times \frac{\partial \mathbf{w}^*(\boldsymbol{\lambda})}{\partial \boldsymbol{\lambda}}}_{\text{indirect grad.}} \quad (9)$$

Following the standard convention in gradient-based hyperparameter optimization (Bengio, 2000; Franceschi et al., 2018), the validation loss  $\mathcal{L}_V$  is typically defined as the task-specific performance (e.g., cross-entropy) on a held-out set using the optimized weights  $\mathbf{w}^*$ . Crucially, in our formulation, the adaptive node scores  $\boldsymbol{\lambda}$  serve as selection or weighting coefficients during the training phase to guide the LLM query process, but they do not explicitly appear in the architectural definition or the loss objective of the validation stage.

Consequently, the direct gradient term  $\partial \mathcal{L}_V / \partial \boldsymbol{\lambda}$  vanishes identically. This classifies our objective as a “pure-response” game (Lorraine et al., 2020), where the hyperparameters influence the outer objective solely by shifting the inner-level equilibrium  $\mathbf{w}^*(\boldsymbol{\lambda})$  (Pedregosa, 2016). This formulation is widely adopted in large-scale bilevel problems to reduce computational complexity without loss of theoretical rigor, as the coupling between  $\boldsymbol{\lambda}$  and  $\mathcal{L}_V$  is entirely captured by

the indirect gradient (Liu et al., 2022). With the hypergradient reduced to this indirect component, we leverage the Implicit Function Theorem (IFT) to explicitly address this non-trivial dependency.

**Theorem 2.1** (Implicit Function Theorem (IFT) Solution). *If for a given hyperparameter  $\boldsymbol{\lambda}'$ , the model parameters  $\mathbf{w}' = \mathbf{w}^*(\boldsymbol{\lambda}')$  satisfy the stationarity condition*

$$\frac{\partial \mathcal{L}_T}{\partial \mathbf{w}} \Big|_{(\boldsymbol{\lambda}', \mathbf{w}')} = 0,$$

*and the training Hessian  $\mathbf{H}_{\mathbf{w}\mathbf{w}} := \frac{\partial^2 \mathcal{L}_T}{\partial \mathbf{w} \partial \mathbf{w}^T}$  is invertible at  $(\boldsymbol{\lambda}', \mathbf{w}')$ , then the best-response function  $\mathbf{w}^*(\boldsymbol{\lambda})$  is implicitly defined and differentiable in a neighborhood of  $\boldsymbol{\lambda}'$ . Its Jacobian is*

$$\frac{\partial \mathbf{w}^*}{\partial \boldsymbol{\lambda}} \Big|_{\boldsymbol{\lambda}'} = - \lim_{i \rightarrow \infty} \sum_{j=0}^i \left( I - \frac{\partial^2 \mathcal{L}_T}{\partial \mathbf{w} \partial \mathbf{w}^T} \right)^j \times \frac{\partial^2 \mathcal{L}_T}{\partial \mathbf{w} \partial \boldsymbol{\lambda}^T} \Big|_{\boldsymbol{\lambda}', \mathbf{w}^*(\boldsymbol{\lambda}')} \quad (10)$$

The proof can be found in Appendix A. Detailed steps to approximate hypergradient computation are as Algorithm 2.

Although the hypergradient updates continuous scores  $\boldsymbol{\lambda}$ , the actual sparse querying requires a binary mask  $\mathbf{m} \in \{0, 1\}^N$ . A naive continuous relaxation (e.g., Gumbel-Softmax) fails to reduce costs, as the expectation-based loss definition  $\sum_n \lambda_n \cdot \ell_n(\hat{y}_n, y_n)$  inherently requires evaluating every node in the graph. To achieve genuine efficiency, we employ a Straight-Through Estimator (STE) via the stop-gradient trick, the detailed procedure of which is illustrated in Algorithm 3. This allows the forward pass to perform a hard  $K$ -hot discrete selection, effectively pruning  $(N - K)$  nodes and minimizing expensive operations (e.g., LLM queries). To ensure stable gradient estimation, we scale the softmax probability vector  $\mathbf{p}$  by  $K$ , aligning its magnitude with the  $K$ -hot mask  $\mathbf{h}$  (where  $\sum h_i = K$ ). This ensures the framework is both computationally sparse and end-to-end differentiable (Kool et al., 2019). Formally:

$$\mathbf{m} = K \cdot \mathbf{p} + \text{stop\_gradient}(\mathbf{h} - K \cdot \mathbf{p}) \quad (11)$$

where  $\mathbf{h}$  is the discrete  $K$ -hot mask obtained via Top- $K$  sampling, and  $\mathbf{p}$  is the softmax probability vector (where  $\sum p_i = 1$ ). During the forward pass, the stop-gradient operation ensures  $\mathbf{m} = \mathbf{h}$ , restricting computation to selected samples only. During the backward pass, the gradient  $\frac{\partial \mathbf{m}}{\partial \boldsymbol{\lambda}}$  is approximated by  $\frac{\partial (K \cdot \mathbf{p})}{\partial \boldsymbol{\lambda}}$ , providing a smooth and informative signal for optimization.

### 2.4. Advantages over Alternative Approaches

Existing approaches face a scalability bottleneck as their cost scales linearly with node count ( $O(N \cdot C_{\text{LLM}})$ ) (He et al., 2024; Zhu et al., 2024), making them impractical

**Algorithm 1** Bilevel-Optimized Sparse Querying

---

```

1: Input: initial node importance scores  $\lambda$ , temperature
    $\tau$ , top- $K$ , outer steps  $T$ , inner steps  $I$ , dataset  $\mathcal{G} =$ 
    $(\mathcal{V}, \mathcal{A}, \{s_n\}_{n \in \mathcal{V}})$ 
2: Output: optimized model parameters  $\mathbf{w}$  and node im-
   portance scores  $\lambda$ 
3: for  $t = 1$  to  $T$  do
4:    $\triangleright$  Differentiable sparse selection
5:    $\mathbf{m} \leftarrow \text{GumbelTopK}(\lambda, \tau, K)$ 
6:    $\triangleright$  Selective LLM querying
7:    $\mathbf{X} \leftarrow \text{SparseQuerying}(\{s_n\}_{n \in \mathcal{V}}, \mathbf{m})$ 
8:    $\triangleright$  Lower-level: Optimize GNN parameters
9:    $\mathbf{w} \leftarrow \text{Initialize}(\cdot)$ 
10:  for  $i = 1$  to  $I$  do
11:     $\mathcal{L}_T \leftarrow \ell(\text{GNN}(\mathbf{X}, \mathcal{A}; \mathbf{w}), \mathbf{Y}_T)$ 
12:    Update  $\mathbf{w}$  by gradient step  $\frac{\partial \mathcal{L}_T}{\partial \mathbf{w}}$ 
13:  end for
14:   $\triangleright$  Upper-level: Optimize selection strategy
15:   $\mathcal{L}_V \leftarrow \ell(\text{GNN}(\mathbf{X}, \mathcal{A}; \mathbf{w}), \mathbf{Y}_V)$ 
16:   $\frac{\partial \mathcal{L}_V}{\partial \lambda} \leftarrow \text{HyperGrad}(\mathcal{L}_V, \mathcal{L}_T, \lambda, \mathbf{w})$ 
17:  Update  $\lambda$  by gradient step  $\frac{\partial \mathcal{L}_V}{\partial \lambda}$ 
18:   $\tau \leftarrow \max(\tau \cdot \gamma, \tau_{\min})$  {Temperature annealing}
19: end for

```

---

for large graphs. In contrast, we introduce a **sparse selective querying mechanism that completely decouples the number of LLM queries from the total node count  $N$** . By capping invocations at a constant budget  $K \ll N$ , our design yields a complexity of  $O(K \cdot C_{\text{LLM}})$ . This drastically reduces overhead compared to whole-graph methods, enabling practical scalability to large graphs where prior methods are infeasible. A formal treatment of time complexity can be found in Appendix D.1. Furthermore, to maintain competitive performance, previous approach (He et al., 2024) necessitates fine-tuning the full LM parameters and operates multi-stream pipelines—maintaining separate fine-tuned LMs and GNNs for the original text and explanations, respectively. This architectural redundancy significantly escalates the per-node computational cost. Conversely, our method freezes the LM parameters and employs a unified single-stream pipeline, eliminating this redundancy to further minimize the resource consumption per node.

Another key strength of our method lies in its ability to **autonomously identify and prioritize the most informative nodes for the specific downstream task**. Unlike heuristic-based baselines that rely on predefined, static metrics to estimate node utility, our framework features a fully differentiable, end-to-end learning process for node selection. This task-driven update mechanism, guided directly by validation feedback, ensures that the limited query budget  $K$  is dynamically allocated to nodes offering the highest marginal utility. Consequently, our approach optimally utilizes the

*Table 1.* Basic dataset statistics. The first three datasets (Photo, Instagram, Computer) are node classification tasks, while the last three (User-ltv, Item-ltv, Post-votes) are node regression tasks. User-ltv and Item-ltv represent different node types (User nodes and Book item nodes, respectively) within the same heterogeneous graph.

Dataset	#Nodes	#Edges	Avg. #Token
Photo	48,362	873,793	182.30
Instagram	11,339	155,349	46.80
Computer	87,229	1,256,548	111.66
User-ltv	35,772	70,632	132.62
Item-ltv	35,772	70,632	132.62
Post-votes	40,947	91,142	154.15

expensive LLM queries, surpassing the performance limitations of fixed, manually designed scoring functions.

### 3. Experiment

In this section, we conduct experiments to evaluate the proposed BOSQ framework on two types of node-level tasks: node classification and node regression. The node classification task involves predicting the class labels of unlabeled nodes given a small set of labeled nodes in a TAG, while the node regression task aims to predict continuous attributes of unlabeled nodes. We begin by describing the experimental settings and then investigate the following research questions: **Q1**: How does BOSQ perform overall on node classification and regression tasks? **Q2**: For large-scale graphs, how significantly does the sparse querying reduce computational overhead? **Q3**: How effective is bilevel optimization at selecting key nodes compared to other approaches, and how much extra computational cost does it incur? **Q4**: How transferable are the learned importance scores across different scale GNN architectures?

#### 3.1. Experimental Setup

**Datasets.** We evaluate our method on six real-world text-attributed graph datasets covering node classification (Instagram, Photo, Computer – homogeneous graphs from (Wu et al., 2025)) and node regression (User-ltv, Item-ltv, Post-votes – heterogeneous graphs from (Robinson et al., 2024), with downsampling applied due to the large original size). Basic dataset statistics including number of nodes and edges, average token count are summarized in Table 1. Detailed information and dataset splitting methods are presented in Appendix B. Unless otherwise specified, all reported time metrics refer to the total end-to-end execution time, covering preprocessing, training, and testing stages.

**Baselines.** To evaluate the effectiveness of our proposed BOSQ, we compare it against a diverse set of baselines covering traditional GNNs, pretrained language models, and LLM-augmented graph methods. For the node classification

task, we employ twelve baselines including the classical GNN models GCN (Kipf & Welling, 2017), SAGE (Hamilton et al., 2017), and GAT (Veličković et al., 2018); pre-trained language models SentenceBERT-66M(Reimers & Gurevych, 2019), RoBERTa-355M(Liu et al., 2019), and BERT(Devlin et al., 2019); state-of-the-art LLM-based textual graph learning methods TAPE (He et al., 2024), ENGINE(Zhu et al., 2024), and LLaGA(Chen et al., 2024); as well as GCN variants enhanced with LLM-derived features, namely LLMEmb and LLMExpl. Furthermore, we include LLMPred, a pure LLM instruction-tuning approach that fine-tunes the LLM to directly predict labels without a GNN component. For the node regression task, following the RelBench benchmark where the graph is heterogeneous, we adopt the corresponding heterogeneous graph versions of GNNs (HeteroGCN, HeteroSAGE, HeteroGAT) and their LLM-enhanced variants (LLMEmb, LLMEExpl). Our method (*ours*) is evaluated under the same settings for both tasks. To ensure fair comparison, all experiments are run on the same local machine using self-hosted LLMs to eliminate API-induced variances. Implementation details and hyperparameter settings are provided in Appendix C.

### 3.2. Overall Performance Comparison (Q1)

We evaluate BOSQ across six real-world TAG datasets involving node classification and node regression tasks, with results summarized in Table 2 and Table 3. Our empirical results demonstrate that BOSQ achieves up to a **167.9 × speedup** over existing GraphLLM methods while consistently delivering **on-par or superior performance**.

**Comparison with Traditional Baselines:** This category includes traditional GNNs (GCN, SAGE, GAT) and pre-trained language models (BERT, RoBERTa, SenBERT). *Observation 1: Traditional GNNs are efficient but suffer from limited semantic depth.* While models like GraphSAGE and GAT exhibit the lowest runtimes (averaging under 17s), their accuracy on classification tasks is significantly lower than LLM-augmented methods, with a gap exceeding 5% on datasets like *Computer*. This indicates that shallow features cannot fully capture the complex attributes in TAGs. *Observation 2: BOSQ outperforms PLM-based features in both accuracy and efficiency.* Surprisingly, PLMs like RoBERTa and BERT require substantial processing time (e.g., 1832.97s for RoBERTa) without yielding competitive results. In contrast, BOSQ is not only faster but also provides a significant boost in predictive power by leveraging LLM-derived explanations rather than raw embeddings. For instance, in regression tasks, BOSQ reduces the average MAE from 6.39 (HeteroGAT) to 5.40, demonstrating the necessity of high-level reasoning.

**Comparison with LLM-based Methods:** We compare BOSQ against state-of-the-art GraphLLM frameworks, in-

cluding TAPE, ENGINE, LLaGA, and several LLM-based baselines. *Observation 3: BOSQ resolves the computational bottleneck of LLM-augmented graph mining.* Representative methods like TAPE and LLMExpl are severely limited by the cost of repeated LLM queries, requiring over 100,000 seconds for medium-sized benchmarks. BOSQ achieves a **167.9 × speedup** over TAPE while maintaining identical accuracy. This proves that our adaptive sparse querying strategy successfully avoids redundant computations without sacrificing the "LLM gain". *Observation 4: Superior performance in regression tasks through sparse optimization.* As shown in Table 3, BOSQ achieves the **best MAE (Rank 1)** on every regression dataset. Unlike LLMExpl, which queries all nodes, our bilevel-optimized querying selectively identifies nodes where LLM insights are most beneficial. This sparse strategy not only saves time but also filters out potentially noisy or low-gain textual information, leading to more precise numerical predictions. *Observation 5: Practicality and Scalability.* While efficiency-focused models like ENGINE and LLaGA reduce runtime to some extent, BOSQ remains the fastest among all LLM-based competitors (ranking 1st in speed in both Table 2 and Table 3). By bringing the total runtime down to a magnitude comparable to standard GNN training, BOSQ stands out as the most viable framework for deploying GraphLLM in real-world, large-scale scenarios.

### 3.3. Scaling up to Million-Scale Graph (Q2)

To evaluate the practical scalability of BOSQ, we conduct experiments on the *ogbn-products* dataset from the Open Graph Benchmark (OGB) (Hu et al., 2020). This is a large-scale text-attributed graph comprising over 2.4 million nodes and 123.7 million edges, with an average of 145.50 tokens per node, posing a significant computational challenge for LLM-based methods. To ensure a representative comparison, we select the most efficient baselines from each category: GCN and SenBERT as classic GNN and LM-based methods, and LLaGA, LLMExpl, and LLMEmb as representative GraphLLM frameworks.

The results, summarized in Table 4, reveal a stark contrast in efficiency. While classic methods (GCN, SenBERT) are computationally efficient, their performance is limited by the lack of high-level reasoning. Conversely, existing GraphLLM methods, despite their potential, become computationally intractable at this scale, failing to complete within a 24-hour time limit due to the exhaustive nature of their LLM querying or embedding processes. In contrast, BOSQ successfully processes the entire graph in just 7.4 hours, achieving the highest accuracy of 78.42%. This demonstrates that our bilevel-optimized sparse querying strategy effectively breaks the scalability bottleneck, making LLM-enhanced graph learning viable for industrial-scale applications.

Table 2. Performance comparison on node classification tasks with Accuracy (%) and Total Time (s) reported. The **best** and second-best accuracy results, as well as the **fastest** and **second-fastest** times, are highlighted.

Methods	Photo		Instagram		Computer		Average	
	time (s) ↓	acc ↑	time (s) ↓	acc ↑	time (s) ↓	acc	time (s) ↓	acc ↑
GCN	15.15	70.63 $\pm$ 0.71	1.78	63.32 $\pm$ 0.22	21.47	71.70 $\pm$ 0.77	12.80	68.55
SAGE	15.62	76.44 $\pm$ 0.23	1.72	63.22 $\pm$ 0.41	21.67	80.33 $\pm$ 0.47	13.00	73.33
GAT	18.05	79.63 $\pm$ 0.39	2.27	63.39 $\pm$ 0.22	27.86	81.93 $\pm$ 1.40	16.06	74.98
SenBERT	321.44	74.14 $\pm$ 0.18	40.08	62.71 $\pm$ 0.58	578.36	70.34 $\pm$ 0.25	313.29	69.06
RoBERTa	1,787.73	75.15 $\pm$ 0.34	427.19	65.33 $\pm$ 0.37	3,283.98	71.02 $\pm$ 0.61	1832.97	70.50
BERT	637.51	73.11 $\pm$ 0.09	71.98	62.55 $\pm$ 0.39	1,162.61	68.35 $\pm$ 0.62	624.03	68.00
TAPE	120,802.00	<b>85.79<math>\pm</math>0.13</b>	31,475.80	65.74 $\pm$ 1.25	149,887.00	<b>89.73<math>\pm</math>0.06</b>	100721.60	<b>80.42</b>
ENGINE	2,613.60	84.78 $\pm$ 0.20	536.01	67.09 $\pm$ 0.38	4,196.57	87.06 $\pm$ 0.23	2448.73	79.64
LLaGA	4,288.58	84.66 $\pm$ 0.17	581.77	64.85 $\pm$ 1.17	7,445.99	88.02 $\pm$ 0.49	4105.45	79.18
LLMExpl	116,157.00	84.97 $\pm$ 0.25	30,737.90	64.94 $\pm$ 0.24	144,291.00	88.39 $\pm$ 0.10	97061.97	79.43
LLMEmb	2,077.30	85.35 $\pm$ 0.24	334.94	<b>67.21<math>\pm</math>0.34</b>	3,293.02	88.60 $\pm$ 0.15	1901.75	80.39
LLMPred	13,515.00	73.69 $\pm$ 0.37	11,794.40	43.69 $\pm$ 0.69	29,592.80	70.39 $\pm$ 0.12	18300.73	62.59
ours	<b>490.55</b>	85.75 $\pm$ 0.28	<b>129.04</b>	66.22 $\pm$ 0.55	<b>1,180.41</b>	89.30 $\pm$ 0.11	<b>600.00</b>	<b>80.42</b>

Table 3. Performance comparison on node regression tasks with Mean Absolute Error (MAE) and Total Time (s) reported. The **best** and second-best MAE results, as well as the **fastest** and **second-fastest** times, are highlighted.

Methods	User-ltv		Item-ltv		Post-votes		Average	
	time (s) ↓	mae ↓	time (s) ↓	mae ↓	time (s) ↓	mae ↓	time (s) ↓	mae ↓
HeteroGCN	13.71	1.39 $\pm$ 0.06	13.67	17.67 $\pm$ 0.29	15.77	0.11 $\pm$ 0.03	14.38	6.39
HeteroSAGE	13.82	1.37 $\pm$ 0.01	13.77	17.77 $\pm$ 0.30	16.18	0.12 $\pm$ 0.04	14.59	6.42
HeteroGAT	13.74	1.39 $\pm$ 0.06	13.68	17.67 $\pm$ 0.29	15.76	0.11 $\pm$ 0.03	14.39	6.39
LLMEmb	1,430.20	1.35 $\pm$ 0.03	1,434.41	15.64 $\pm$ 0.19	1,713.90	0.10 $\pm$ 0.03	1526.17	5.70
LLMExpl	32,672.90	1.34 $\pm$ 0.03	34,600.20	15.40 $\pm$ 0.07	32,230.40	0.09 $\pm$ 0.03	33167.83	5.61
ours	<b>419.03</b>	<b>1.33<math>\pm</math>0.02</b>	<b>421.62</b>	<b>14.79<math>\pm</math>0.01</b>	<b>494.32</b>	<b>0.08<math>\pm</math>0.02</b>	<b>444.99</b>	<b>5.40</b>

Table 4. Scalability and efficiency analysis on the million-scale ogbn-products dataset. ‘—’ indicates the method exceeded the 24-hour time limit. BOSQ achieves the best accuracy while remaining computationally feasible.

Methods	Accuracy (%)	Time (hrs)	Efficiency
GCN	69.01	0.1	✓
SenBERT	77.10	2.9	✓
LLaGA	—	> 24	✗
LLMExpl	—	> 24	✗
LLMEmb	—	> 24	✗
Ours	<b>78.42</b>	<b>7.4</b>	✓

#### 3.4. Ablation Study of Sparse Selection Strategy (Q3)

To address **Q3**, we evaluate the effectiveness of our proposed bilevel-optimized selection strategy in identifying the most informative nodes for LLM querying. Specifically, we compare our approach against three representative baselines: 1) *Random Selection*: A fixed budget of  $K$  nodes is selected uniformly at random from the graph. 2) *Heuristic (Local Dissimilarity)*: This strategy prioritizes “information-deficient” nodes that exhibit high semantic dissimilarity to their neighbors. The score is defined as the cosine distance between a node’s feature  $\mathbf{h}_n$  and its neighborhood mean

feature  $\mathbf{h}_n^N = \frac{1}{|\mathcal{N}(n)|} \sum_{m \in \mathcal{N}(n)} \mathbf{h}_m$ . Node with the highest dissimilarity are selected:  $\text{Score}_n^{\text{dissim}} = 1 - \frac{\mathbf{h}_n \cdot \mathbf{h}_n^N}{\|\mathbf{h}_n\| \|\mathbf{h}_n^N\|}$ . 3) *Heuristic (Prediction Entropy)*: This strategy targets nodes where the base model is most uncertain. We compute the normalized entropy of the prediction logits for each node. Nodes with the highest entropy are selected:  $\text{Score}_n^{\text{ent}} = -\frac{\sum_{c=1}^C p_{n,c} \log p_{n,c}}{\log C}$ . where  $p_{n,c}$  is the softmax probability for class  $c$  and  $C$  is the number of classes.

We maintain identical hyperparameters (budget  $K$ , model architecture, and other settings) across all strategies. The node classification accuracy and total training time on the Instagram and Photo dataset are reported in Table 5. As shown in the results, while heuristic-based methods like Prediction Entropy provide a stronger baseline than Random selection by focusing on uncertain regions, our bilevel strategy consistently achieves the highest accuracy. This superiority stems from its ability to account for the complex interaction between node features and graph topology, rather than relying on isolated local or predictive signals. Comprehensive performance and complexity analyses in Appendix D.2 further demonstrate that our bilevel selection

dynamically prioritizes task-critical nodes with negligible computational overhead relative to the dominant cost of LLM inference.

**Table 5. Ablation study of the node selection strategy in BOSQ.** We compare our bilevel-optimized sparse querying against random selection, prediction entropy, and a local dissimilarity heuristic. Our approach yields the best performance with marginal time overhead.

Selection Strategy	Instagram		Photo	
	Accuracy (%) $\uparrow$	Time (s) $\downarrow$	Accuracy (%) $\uparrow$	Time (s) $\downarrow$
Random	65.68 $\pm$ 0.37	125.26	85.61 $\pm$ 0.32	393.11
Local Dissimilarity	65.89 $\pm$ 0.69	110.27	85.62 $\pm$ 0.22	370.83
Prediction Entropy	65.82 $\pm$ 0.47	141.02	85.54 $\pm$ 0.34	380.76
Ours (Bilevel-Optimized)	66.22 $\pm$ 0.55	129.04	85.75 $\pm$ 0.28	490.55

### 3.5. Transferability of Importance Scores (Q4)

To address **Q4**, we conduct a cross-evaluation on the Instagram dataset using two GCN architectures with a 225.5 $\times$  complexity gap: a Small 1-layer model (2,050 parameters) and a Big 5-layer model with 256 hidden units (462,338 parameters). Notably, the configurations for both models—specifically the shallow 1-layer and the deep 5-layer structure—fall outside the hyperparameter optimization range used in our primary experiments (Table 2). This setup allows us to test whether importance scores learned on a restricted proxy can generalize to a much larger target model under extreme architectural shifts. As shown in Table 6, node selections optimized on the Small proxy model consistently yield superior results when transferred to the Big target model (66.37% accuracy) compared to the selection optimized directly on the Big model itself (66.20%). A similar trend is observed when evaluating on the Small target model, where the Small-source selection maintains a slight performance edge. We provide an in-depth analysis in Appendix D.3, showing that our shallow proxy choice effectively preserves node distinctiveness and enhances the quality of importance scores for the downstream tasks.

**Table 6. Transferability analysis and efficiency of node selection.** We report the Accuracy (%) on different **Target** models using node selections optimized on different **Source** models. The #Params column indicates the model complexity used during the bilevel optimization.

Selection Source	#Params	Target: Small	Target: Big
Source: Small	2,050	65.89 $\pm$ 0.23	66.37 $\pm$ 0.67
Source: Big	462,338	65.85 $\pm$ 0.44	66.20 $\pm$ 0.17
Efficiency Gain	225.5 $\times$	+0.04	+0.17

## 4. Related Works

**Graph Neural Networks.** GNNs (Kipf & Welling, 2017; Veličković et al., 2018) are standard for graph learning via message passing. For TAGs, node features have evolved from shallow features to PLM-based embeddings (Devlin et al., 2019; Liu et al., 2019). While methods like GLEM (Zhao et al., 2023) and PATTON (Jin et al., 2023) enhance PLM-GNN interaction. However, as noted in previ-

ous studies (He et al., 2024; Zhu et al., 2024), these methods also suffer from prohibitive computational overhead problem.

**Graph with Large Language Models.** Existing GraphLLM methods for node-level tasks fall into three categories based on LLM roles (Wu et al., 2025): (1) LLM as predictor, linearizing entire graphs for direct LLM predictions (e.g., LLaGA (Chen et al., 2024), GraphGPT (Tang et al., 2024)); (2) LLM as encoder, jointly embedding node text and context (e.g., ENGINE (Zhu et al., 2024)); (3) LLM as explainer (our focus), where LLMs provide auxiliary explanation features to enhance GNN inputs (e.g., TAPE (He et al., 2024)). However, these approaches typically query LLMs for all nodes, incurring prohibitive computational cost. In contrast, our BOSQ framework introduces a *selective querying* mechanism to adaptively identify a sparse subset of nodes worth querying, significantly improving efficiency without sacrificing task performance.

**Bilevel Optimization in Machine Learning.** Bilevel optimization addresses problems with nested structure, where an outer-level objective depends on the solution to an inner-level optimization (Zhang et al., 2024). It is widely applied in hyperparameter tuning (Lorraine et al., 2020) and meta-learning (e.g., MAML (Finn et al., 2017)). We pioneer the use of bilevel optimization in the *efficient GraphLLM* domain, focusing on selective LLM querying in graphs. This formulation directly aligns query selection with task utility and inherently promotes sparsity, addressing both efficiency and effectiveness.

**Node-level Tasks on TAGs.** Most existing works on TAGs focus primarily on *node classification*, assigning discrete labels to nodes, which has become the classical and dominant benchmark in this area (Chen et al., 2022; 2025; Deng et al., 2024). However, with the growing interest in representation learning for Relational Deep Learning tasks, *node regression*—predicting continuous node attributes—has attracted increasing attention due to its practical relevance in domains such as e-commerce systems (Robinson et al., 2024). To validate the generality of BOSQ, we conduct experiments on both task types across diverse real-world TAG datasets.

## 5. Conclusion

In this paper, we proposed BOSQ, an efficient framework that overcomes the scalability bottleneck of GraphLLMs via a bilevel-optimized sparse querying strategy. By selectively invoking LLMs for only the most task-critical nodes, BOSQ achieves orders of magnitude speedup over current methods while consistently delivering on-par or superior performance across classification and regression tasks. Our extensive evaluations demonstrate that BOSQ is scalable to million-node graphs, providing a practical solution for the efficient deployment of GraphLLMs.

## Impact Statement

This paper presents work whose goal is to advance the field of Machine Learning. There are many potential societal consequences of our work, none which we feel must be specifically highlighted here.

## References

Bengio, Y. Gradient-Based Optimization of Hyperparameters. *Neural Comput.*, 12(8):1889–1900, August 2000. ISSN 0899-7667. doi: 10.1162/089976600300015187.

Bengio, Y. The consciousness prior. *arXiv preprint arXiv:1709.08568*, 2017.

Chen, J., Gao, K., Li, G., and He, K. NAGphomer: A Tokenized Graph Transformer for Node Classification in Large Graphs. In *The Eleventh International Conference on Learning Representations*, September 2022.

Chen, J., Li, C., Li, G., Hopcroft, J. E., and He, K. Rethinking Tokenized Graph Transformers for Node Classification, February 2025.

Chen, R., Zhao, T., Jaiswal, A. K., Shah, N., and Wang, Z. LLaGA: Large Language and Graph Assistant. In *Forty-First International Conference on Machine Learning, ICML 2024, Vienna, Austria, July 21-27, 2024*. OpenReview.net, 2024.

Deng, C., Yue, Z., and Zhang, Z. Polynormer: Polynomial-Expressive Graph Transformer in Linear Time. In *The Twelfth International Conference on Learning Representations, ICLR 2024, Vienna, Austria, May 7-11, 2024*. OpenReview.net, 2024.

Devlin, J., Chang, M.-W., Lee, K., and Toutanova, K. BERT: Pre-training of Deep Bidirectional Transformers for Language Understanding. In *Proceedings of the 2019 Conference of the North*, pp. 4171–4186, Minneapolis, Minnesota, 2019. Association for Computational Linguistics. doi: 10.18653/v1/N19-1423.

Fang, Y., Li, X., Pan, Y., Huang, X., and Tsang, I. W. Boosting with Fewer Tokens: Multi-Query Optimization for LLMs Using Node Text and Neighbor Cues. In *2025 IEEE 41st International Conference on Data Engineering (ICDE)*, pp. 2684–2697, May 2025. doi: 10.1109/ICDE65448.2025.00202.

Finn, C., Abbeel, P., and Levine, S. Model-agnostic meta-learning for fast adaptation of deep networks. In *Proceedings of the 34th International Conference on Machine Learning - Volume 70*, ICML’17, pp. 1126–1135, Sydney, NSW, Australia, August 2017. JMLR.org.

Franceschi, L., Frasconi, P., Salzo, S., Grazzi, R., and Pontil, M. Bilevel Programming for Hyperparameter Optimization and Meta-Learning. In Dy, J. G. and Krause, A. (eds.), *Proceedings of the 35th International Conference on Machine Learning, ICML 2018, Stockholmsmässan, Stockholm, Sweden, July 10-15, 2018*, volume 80 of *Proceedings of Machine Learning Research*, pp. 1563–1572. PMLR, 2018.

Gao, L., Rajaram, A., Coxon, J., Govande, S. V., Baker, B., and Mossing, D. Weight-sparse transformers have interpretable circuits. *arXiv preprint arXiv:2511.13653*, 2025.

Hamilton, W. L., Ying, R., and Leskovec, J. Inductive representation learning on large graphs. In *Proceedings of the 31st International Conference on Neural Information Processing Systems*, NIPS’17, pp. 1025–1035, Red Hook, NY, USA, December 2017. Curran Associates Inc. ISBN 978-1-5108-6096-4.

He, X., Bresson, X., Laurent, T., Perold, A., LeCun, Y., and Hooi, B. Harnessing Explanations: LLM-to-LM Interpreter for Enhanced Text-Attributed Graph Representation Learning. In *The Twelfth International Conference on Learning Representations, ICLR 2024, Vienna, Austria, May 7-11, 2024*. OpenReview.net, 2024.

Hu, W., Fey, M., Zitnik, M., Dong, Y., Ren, H., Liu, B., Catasta, M., and Leskovec, J. Open graph benchmark: Datasets for machine learning on graphs. In *Proceedings of the 34th International Conference on Neural Information Processing Systems*, NIPS ’20, pp. 22118–22133, Red Hook, NY, USA, December 2020. Curran Associates Inc. ISBN 978-1-7138-2954-6.

Huang, X., Han, K., Yang, Y., Bao, D., Tao, Q., Chai, Z., and Zhu, Q. Can GNN be Good Adapter for LLMs? In *Proceedings of the ACM Web Conference 2024*, pp. 893–904, Singapore Singapore, May 2024. ACM. ISBN 979-8-4007-0171-9. doi: 10.1145/3589334.3645627.

Jin, B., Zhang, W., Zhang, Y., Meng, Y., Zhang, X., Zhu, Q., and Han, J. Patton: Language Model Pretraining on Text-Rich Networks. In Rogers, A., Boyd-Graber, J. L., and Okazaki, N. (eds.), *Proceedings of the 61st Annual Meeting of the Association for Computational Linguistics (Volume 1: Long Papers)*, ACL 2023, Toronto, Canada, July 9-14, 2023, pp. 7005–7020. Association for Computational Linguistics, 2023. doi: 10.18653/V1/2023.ACL-LONG.387.

Kipf, T. N. and Welling, M. Semi-Supervised Classification with Graph Convolutional Networks. In *International Conference on Learning Representations*, February 2017.

Kool, W., van Hoof, H., and Welling, M. Estimating Gradients for Discrete Random Variables by Sampling without Replacement. In *International Conference on Learning Representations*, September 2019.

Li, Y., Wang, P., Zhu, X., Chen, A., Jiang, H., Cai, D., Chan, W. K. V., and Li, J. GLBench: A Comprehensive Benchmark for Graph with Large Language Models. In Globersons, A., Mackey, L., Belgrave, D., Fan, A., Paquet, U., Tomczak, J. M., and Zhang, C. (eds.), *Advances in Neural Information Processing Systems 38: Annual Conference on Neural Information Processing Systems 2024, NeurIPS 2024, Vancouver, BC, Canada, December 10 - 15, 2024*, 2024.

Liu, R., Gao, J., Zhang, J., Meng, D., and Lin, Z. Investigating Bi-Level Optimization for Learning and Vision From a Unified Perspective: A Survey and Beyond. *IEEE Transactions on Pattern Analysis and Machine Intelligence*, 44(12):10045–10067, December 2022. ISSN 0162-8828, 2160-9292, 1939-3539. doi: 10.1109/TPAMI.2021.3132674.

Liu, Y., Ott, M., Goyal, N., Du, J., Joshi, M., Chen, D., Levy, O., Lewis, M., Zettlemoyer, L., and Stoyanov, V. RoBERTa: A Robustly Optimized BERT Pretraining Approach, July 2019.

Lorraine, J., Vicol, P., and Duvenaud, D. Optimizing Millions of Hyperparameters by Implicit Differentiation. In Chiappa, S. and Calandra, R. (eds.), *The 23rd International Conference on Artificial Intelligence and Statistics, AISTATS 2020, 26-28 August 2020, Online [Palermo, Sicily, Italy]*, volume 108 of *Proceedings of Machine Learning Research*, pp. 1540–1552. PMLR, 2020.

Lu, E., Jiang, Z., Liu, J., Du, Y., Jiang, T., Hong, C., Liu, S., He, W., Yuan, E., Wang, Y., Huang, Z., Yuan, H., Xu, S., Xu, X., Lai, G., Chen, Y., Zheng, H., Yan, J., Su, J., Wu, Y., Zhang, N. Y., Yang, Z., Zhou, X., Zhang, M., and Qiu, J. MoBA: Mixture of Block Attention for Long-Context LLMs, February 2025. URL <https://arxiv.org/abs/2502.13189>. arXiv:2502.13189 [cs].

Ma, Y. and Tang, J. *Deep Learning on Graphs*. Cambridge University Press, Cambridge, 2021. ISBN 978-1-108-83174-1. doi: 10.1017/9781108924184.

Nayab, S., Rossolini, G., Simoni, M., Saracino, A., Buttazzo, G., Manes, N., and Giacomelli, F. Concise Thoughts: Impact of Output Length on LLM Reasoning and Cost, January 2025.

Ni, J., Li, J., and McAuley, J. Justifying Recommendations using Distantly-Labeled Reviews and Fine-Grained Aspects. In Inui, K., Jiang, J., Ng, V., and Wan, X. (eds.), *Proceedings of the 2019 Conference on Empirical Methods in Natural Language Processing and the 9th International Joint Conference on Natural Language Processing (EMNLP-IJCNLP)*, pp. 188–197, Hong Kong, China, November 2019. Association for Computational Linguistics. doi: 10.18653/v1/D19-1018.

Pedregosa, F. Hyperparameter optimization with approximate gradient. In *Proceedings of The 33rd International Conference on Machine Learning*, pp. 737–746. PMLR, June 2016.

Posner, M. I. Orienting of attention. *Quarterly journal of experimental psychology*, 32(1):3–25, 1980.

Reimers, N. and Gurevych, I. Sentence-BERT: Sentence Embeddings using Siamese BERT-Networks. In Inui, K., Jiang, J., Ng, V., and Wan, X. (eds.), *Proceedings of the 2019 Conference on Empirical Methods in Natural Language Processing and the 9th International Joint Conference on Natural Language Processing (EMNLP-IJCNLP)*, pp. 3982–3992, Hong Kong, China, November 2019. Association for Computational Linguistics. doi: 10.18653/v1/D19-1410.

Robinson, J., Ranjan, R., Hu, W., Huang, K., Han, J., Dobles, A., Fey, M., Lenssen, J. E., Yuan, Y., Zhang, Z., He, X., and Leskovec, J. RelBench: A Benchmark for Deep Learning on Relational Databases. In Globersons, A., Mackey, L., Belgrave, D., Fan, A., Paquet, U., Tomczak, J. M., and Zhang, C. (eds.), *Advances in Neural Information Processing Systems 38: Annual Conference on Neural Information Processing Systems 2024, NeurIPS 2024, Vancouver, BC, Canada, December 10 - 15, 2024*, 2024.

Tang, J., Yang, Y., Wei, W., Shi, L., Su, L., Cheng, S., Yin, D., and Huang, C. GraphGPT: Graph Instruction Tuning for Large Language Models. In Yang, G. H., Wang, H., Han, S., Hauff, C., Zuccon, G., and Zhang, Y. (eds.), *Proceedings of the 47th International ACM SIGIR Conference on Research and Development in Information Retrieval, SIGIR 2024, Washington DC, USA, July 14-18, 2024*, pp. 491–500. ACM, 2024. doi: 10.1145/3626772.3657775.

Touvron, H., Lavril, T., Izacard, G., Martinet, X., Lachaux, M.-A., Lacroix, T., Rozière, B., Goyal, N., Hambro, E., Azhar, F., Rodriguez, A., Joulin, A., Grave, E., and Lample, G. LLaMA: Open and Efficient Foundation Language Models, February 2023.

Veličković, P., Cucurull, G., Casanova, A., Romero, A., Liò, P., and Bengio, Y. Graph Attention Networks. In *International Conference on Learning Representations*, February 2018.

Wu, X., Shen, Y., Ge, F., Shan, C., Jiao, Y., Sun, X., and Cheng, H. When Do LLMs Help With Node Classification? A Comprehensive Analysis. In *Forty-Second International Conference on Machine Learning, ICML 2025, Vancouver, BC, Canada, July 13-19, 2025*. OpenReview.net, 2025.

Yuan, J., Gao, H., Dai, D., Luo, J., Zhao, L., Zhang, Z., Xie, Z., Wei, Y., Wang, L., Xiao, Z., Wang, Y., Ruan, C., Zhang, M., Liang, W., and Zeng, W. Native Sparse Attention: Hardware-Aligned and Natively Trainable Sparse Attention. In Che, W., Nabende, J., Shutova, E., and Pilehvar, M. T. (eds.), *Proceedings of the 63rd Annual Meeting of the Association for Computational Linguistics (Volume 1: Long Papers)*, pp. 23078–23097, Vienna, Austria, July 2025. Association for Computational Linguistics. ISBN 979-8-89176-251-0. doi: 10.18653/v1/2025.acl-long.1126. URL <https://aclanthology.org/2025.acl-long.1126/>.

Zhang, Y., Khanduri, P., Tsaknakis, I., Yao, Y., Hong, M., and Liu, S. An Introduction to Bilevel Optimization: Foundations and applications in signal processing and machine learning. *IEEE Signal Processing Magazine*, 41(1):38–59, April 2024. ISSN 1053-5888, 1558-0792. doi: 10.1109/MSP.2024.3358284.

Zhao, J., Qu, M., Li, C., Yan, H., Liu, Q., Li, R., Xie, X., and Tang, J. Learning on Large-scale Text-attributed Graphs via Variational Inference. In *The Eleventh International Conference on Learning Representations, ICLR 2023, Kigali, Rwanda, May 1-5, 2023*. OpenReview.net, 2023.

Zhu, Y., Wang, Y., Shi, H., and Tang, S. Efficient Tuning and Inference for Large Language Models on Textual Graphs. In *Proceedings of the Thirty-Third International Joint Conference on Artificial Intelligence, IJCAI 2024, Jeju, South Korea, August 3-9, 2024*, pp. 5734–5742. ijcai.org, 2024.

## A. IFT proof

**Theorem A.1** (Implicit Function Theorem (IFT) Solution). *If for a given hyperparameter  $\lambda'$ , the model parameters  $\mathbf{w}' = \mathbf{w}^*(\lambda')$  satisfy the stationarity condition*

$$\frac{\partial \mathcal{L}_T}{\partial \mathbf{w}} \Big|_{(\lambda', \mathbf{w}')} = 0,$$

*and the training Hessian  $\mathbf{H}_{\mathbf{w}\mathbf{w}} := \frac{\partial^2 \mathcal{L}_T}{\partial \mathbf{w} \partial \mathbf{w}^T}$  is invertible at  $(\lambda', \mathbf{w}')$ , then the best-response function  $\mathbf{w}^*(\lambda)$  is implicitly defined and differentiable in a neighborhood of  $\lambda'$ . Its Jacobian is*

$$\frac{\partial \mathbf{w}^*}{\partial \lambda} \Big|_{\lambda'} = - \lim_{i \rightarrow \infty} \sum_{j=0}^i \left( I - \frac{\partial^2 \mathcal{L}_T}{\partial \mathbf{w} \partial \mathbf{w}^T} \right)^j \times \frac{\partial^2 \mathcal{L}_T}{\partial \mathbf{w} \partial \lambda^T} \Big|_{\lambda', \mathbf{w}^*(\lambda')} \quad (12)$$

*Proof.* Define the vector-valued function

$$F(\lambda, \mathbf{w}) := \frac{\partial \mathcal{L}_T}{\partial \mathbf{w}}(\lambda, \mathbf{w}).$$

By assumption,  $F(\lambda', \mathbf{w}') = 0$ . The Implicit Function Theorem states that if the Jacobian of  $F$  with respect to  $\mathbf{w}$  at  $(\lambda', \mathbf{w}')$ , i.e.,

$$J_{\mathbf{w}} F(\lambda', \mathbf{w}') := \frac{\partial F}{\partial \mathbf{w}}(\lambda', \mathbf{w}') = \frac{\partial^2 \mathcal{L}_T}{\partial \mathbf{w} \partial \mathbf{w}^T}(\lambda', \mathbf{w}'),$$

is invertible, then there exists a neighborhood of  $\lambda'$  and a unique differentiable function  $\mathbf{w}^*(\lambda)$  such that

$$F(\lambda, \mathbf{w}^*(\lambda)) = 0.$$

Differentiating this identity with respect to  $\lambda$  yields

$$\frac{\partial F}{\partial \lambda} + \frac{\partial F}{\partial \mathbf{w}} \frac{\partial \mathbf{w}^*}{\partial \lambda} = 0.$$

Solving for the Jacobian of the optimal parameters gives

$$\frac{\partial \mathbf{w}^*}{\partial \lambda} = - \left( \frac{\partial F}{\partial \mathbf{w}} \right)^{-1} \times \frac{\partial F}{\partial \lambda}.$$

Substituting back  $F = \partial \mathcal{L}_T / \partial \mathbf{w}$ , we have:

$$\frac{\partial \mathbf{w}^*}{\partial \lambda} = - \left[ \frac{\partial^2 \mathcal{L}_T}{\partial \mathbf{w} \partial \mathbf{w}^T} \right]^{-1} \times \frac{\partial}{\partial \lambda} \left( \frac{\partial \mathcal{L}_T}{\partial \mathbf{w}} \right).$$

To align with the standard notation in the theorem statement, we note that the matrix  $\frac{\partial}{\partial \lambda} \left( \frac{\partial \mathcal{L}_T}{\partial \mathbf{w}} \right)$  has entries  $\left[ \frac{\partial}{\partial \lambda} \left( \frac{\partial \mathcal{L}_T}{\partial \mathbf{w}} \right) \right]_{i,j} = \frac{\partial^2 \mathcal{L}_T}{\partial w_i \partial \lambda_j}$ . This matrix is commonly denoted by  $\frac{\partial^2 \mathcal{L}_T}{\partial \mathbf{w} \partial \lambda^T}$ . Therefore,

$$\frac{\partial \mathbf{w}^*}{\partial \lambda} = - \left[ \frac{\partial^2 \mathcal{L}_T}{\partial \mathbf{w} \partial \mathbf{w}^T} \right]^{-1} \times \frac{\partial^2 \mathcal{L}_T}{\partial \mathbf{w} \partial \lambda^T}.$$

Since the exact inverse of the Hessian is computationally expensive, it can be approximated by an infinite series:

$$\left[ \frac{\partial^2 \mathcal{L}_T}{\partial \mathbf{w} \partial \mathbf{w}^T} \right]^{-1} = \lim_{i \rightarrow \infty} \sum_{j=0}^i \left( I - \frac{\partial^2 \mathcal{L}_T}{\partial \mathbf{w} \partial \mathbf{w}^T} \right)^j \quad (13)$$

Substitute it into the above equation to get the final result:

$$\frac{\partial \mathbf{w}^*}{\partial \lambda} = - \lim_{i \rightarrow \infty} \sum_{j=0}^i \left( I - \frac{\partial^2 \mathcal{L}_T}{\partial \mathbf{w} \partial \mathbf{w}^T} \right)^j \times \frac{\partial^2 \mathcal{L}_T}{\partial \mathbf{w} \partial \lambda^T}.$$

This completes the proof.  $\square$

## B. Dataset Details

### B.1. Node Classification Datasets

The Ele-Photo (abbreviated as **Photo**) and Ele-Computer (abbreviated as **Computer**) datasets are derived from the Amazon Electronics dataset (Ni et al., 2019), where each node represents an item in either the Photo or Computer category. In these e-commerce networks, edges indicate co-purchase or co-view relationships between items. The associated text for each item comprises product descriptions, such as summaries or user reviews. The classification task involves categorizing these products into fine-grained sub-categories. The **Instagram** dataset, originally released in (Huang et al., 2024), features nodes representing users, with edges denoting social connections such as following relationships. Each Instagram node includes textual features extracted from the user’s profile page introduction. The classification task labels specify whether a user is a commercial or a normal user.

Table 7 summarizes the label space for each dataset.

Table 7. Label Space

Dataset	Label Space
Photo	Lighting & Studio, Bags & Cases, Tripods & Monopods, Flashes, Video Surveillance, Accessories, Binoculars & Scopes, Video, Digital Cameras, Film Photography, Lenses, Underwater Photography
Computer	Computer Accessories & Peripherals, Tablet Accessories, Laptop Accessories, Computers & Tablets, Computer Components, Data Storage, Networking Products, Monitors, Servers, Tablet Replacement Parts
Instagram	Normal User, Commercial User

**Train-Test Split.** We follow a semi-supervised learning setup, where only a small subset of nodes is labeled to imitate real-world scenarios with limited annotation. This setting evaluates the model’s ability to leverage scarce labeled data effectively. Specifically, we adopt a 10% training data split on Instagram, Photo, and Computer datasets, consistent with the experimental protocol used in LLMNodeBed (Wu et al., 2025).

### B.2. Node Regression Datasets

**User-ltv** is derived from the Rel-amazon dataset, which contains comprehensive records of products, users, and reviews on Amazon’s platform focusing on book-related products. Each node represents a user, enriched with textual information from their reviews and purchase history. In this regression task, the objective is to predict the total monetary value (\$) of all products a user will buy and review over the next 3 months. **Item-ltv** is also extracted from the same Rel-amazon subset, where nodes correspond to individual products in the book category. Product nodes include textual features such as product descriptions and user reviews. The regression target is to forecast the total monetary value (\$) of purchases and reviews that each product will receive in the coming 3 months. **Post-votes** originates from the Stack Exchange stats-exchange site. Here, nodes represent individual user posts, accompanied by rich textual content such as raw text in posts and comments, as well as metadata like edit histories and voting records. The regression task *post-votes* aims to predict the number of votes each post will receive in the next 3 months based on its current state and textual information.

**Data Downsampling.** Random downsampling is applied to all three node regression datasets to reduce size while preserving representativity. Isolated nodes caused by this process are subsequently removed to maintain graph connectivity.

**Train-Test Split.** We follow the RelBench (Robinson et al., 2024) temporal splitting scheme: training data includes all records up to the validation timestamp (VAL\_TIMESTAMP), validation data covers from VAL\_TIMESTAMP to the test timestamp (TEST\_TIMESTAMP), and testing data includes all records after TEST\_TIMESTAMP.

The detailed statistics and temporal information of these datasets are summarized in Table 8.

## C. Implementation Details

In this section, we provide the detailed experimental setup, including the hyperparameter search space, model-specific configurations, and the prompting strategy used for LLM querying.

Table 8. Detailed Regression Dataset information

	User-ltv	Item-ltv	Post-votes
# Nodes	35,772	35,772	40,947
# Edges	70,632	70,632	91,142
# node types	3	3	7
# edge types	4	4	22
Start Timestamp	2008-01-01	2008-01-01	2009-02-02
Val Timestamp	2015-10-01	2015-10-01	2020-10-01
Test Timestamp	2016-01-01	2016-01-01	2021-01-01
End Timestamp	2018-09-28	2018-09-28	2023-09-03

### C.1. Hyperparameter settings

**Common Experimental Setup.** To ensure a rigorous and fair evaluation of computational efficiency, all experiments are conducted on a Linux server equipped with a NVIDIA 48GB L40 GPU and an Intel(R) Xeon(R) Platinum 8358 CPU (64 cores). Our code is developed based on LLMNodeBed (Wu et al., 2025). Notably, rather than relying on commercial cloud-based APIs (e.g., GPT-4), which are subject to unpredictable network latency and heterogeneous underlying hardware, we employ locally deployed LLMs for all text generation tasks. This setup guarantees that the reported speedup gains are solely attributable to the algorithmic improvements of our adaptive sparse querying strategy rather than external infrastructure variances. We use the Mistral-7B as the LLM as done in LLMNodeBed.

**Node Classification Task.** We perform a grid search to optimize the performance of each model.

- **GNNs:** The number of GNN layers is searched among  $\{1, 2, 3\}$ , and the hidden dimension is selected from  $\{128, 256\}$ . The learning rate is tuned within  $\{0.005, 0.01\}$ . Following LLMNodeBed, we set the maximum number of training epochs to 500 with an early stopping patience of 100.
- **PLMs:** Due to the high computational cost of performing a grid search for fine-tuning language models, we adopt the default hyperparameters from LLMNodeBed, specifically using 10 epochs and a learning rate of  $2 \times 10^{-5}$ .
- **ENGINE:** Following the original paper, we search for the number of layers in  $\{1, 2, 3\}$ , the hidden dimension in  $\{64, 128\}$ , and the learning rate in  $\{5 \times 10^{-4}, 1 \times 10^{-3}\}$ .
- **TAPE:** We utilize Mistral-7B for explanation generation. To ensure reproducibility and manage computational overhead, we use the pre-generated explanations provided by LLMNodeBed. The total explanation generation time is estimated by multiplying the total token count by the per-token latency measured on our local machine. For the GNN component, we search the number of layers in  $\{2, 3, 4\}$ , hidden dimensions in  $\{128, 256\}$ , and learning rates in  $\{5 \times 10^{-4}, 1 \times 10^{-3}\}$ . The LM (RoBERTa-large, 355M) is fine-tuned using its default parameters.
- **LLaGA:** Following the settings of LLMNodeBed, we adopt the HO templates as the default configuration with the number of hops set to 4. RoBERTa-355M is employed as the text encoder, and the linear projection layer is implemented as a 2-layer MLP with a hidden dimension of 2048. We set the batch size to 64 and the learning rate to  $10^{-4}$ . The number of training epochs is 10 for Instagram and 8 for the larger Computer and Photo datasets.
- **LLMEmb:** This method generates node embeddings by mean-pooling the hidden states from the final layer of the LLM. For the GNN backbone, we perform a grid search over the number of layers in  $\{1, 2, 3\}$ , hidden dimensions in  $\{128, 256\}$ , and learning rates in  $\{0.005, 0.01\}$ .
- **LLMExpl:** This approach concatenates the LLM-generated explanations with the original text attributes and subsequently utilizes a frozen LM (RoBERTa-large, 355M) to encode the augmented text into node embeddings. The GNN backbone’s hyperparameters are tuned across the same search space as LLMEmb: layers in  $\{1, 2, 3\}$ , hidden dimensions in  $\{128, 256\}$ , and learning rates in  $\{0.005, 0.01\}$ .
- **LLMPred:** This baseline corresponds to the LLM Instruction Tuning approach from LLMNodeBed. The method directly fine-tunes the LLM to predict node labels without incorporating any GNN components. We follow the default

hyperparameters specified in LLMNodeBed: the LoRA rank  $r$  is set to 8, and the scaling factor  $\alpha$  is set to 16. We use a dropout ratio of 0.1 and a learning rate of  $10^{-5}$ . For each dataset, the input consists of the node’s original text concatenated with a task-specific prompt designed to guide the LLM in classification, while the expected output is the categorical label. We train the model for 8 epochs on Instagram and 2 epochs on Computer and Photo, adjusting for the larger scale of the latter two datasets.

- **BOSQ (Ours):** For our framework, the GNN backbone’s hyperparameter search space includes the number of layers in  $\{2, 3\}$  and hidden dimensions in  $\{128, 256\}$ , with a fixed learning rate of 0.01. For the bilevel optimization, we search the temperature  $\tau$  within  $\{2.0, 4.0\}$  and the multiplier  $\lambda$ ’s learning rate within  $\{10^{-3}, 10^{-2}\}$ . We fix the sparsity  $k = 10$  and the minimum temperature  $\tau_{min} = 0.5$ . We conduct a sensitivity analysis on the hyperparameter  $k$  in Appendix D.4. The results show that 10 is a reasonable value. Consistent with standard practice, we employ RoBERTa-large (355M) as the default language model to encode text to node embeddings. The outer loop number of iterations  $T$  is set to 3, and the inner loop number of iterations  $I$  is set to 200 and early stopping patience of 50. The Neumann series approximation uses  $i = 10$  steps.

**Node Regression Task.** For regression, the GNN baselines, LLMEmb, and LLMExpl follow the same hyperparameter search space as the node classification task. For BOSQ, we set the sparsity  $k = 10$ , temperature  $\tau = 4.0$ ,  $\tau_{min} = 0.5$ , and the learning rate for  $\lambda$  to 0.005. The GNN backbone hyperparameters are searched over  $\{1, 2, 3\}$  layers,  $\{128, 256\}$  hidden dimensions, and a learning rate range of  $\{0.005, 0.01\}$ .

**Analysis of Text Augmentation Strategy.** In the preliminary stage, we compared two ways to incorporate LLM-derived explanations: (1) concatenating the original text  $s_n$  with the explanation  $e_n$ , and (2) replacing  $s_n$  with  $e_n$ . Our empirical results indicated that direct replacement ( $s'_n \leftarrow e_n$ ) yields superior performance. We speculate that concatenation may introduce noise or redundant information from the raw text, which could dilute the task-specific signals present in the LLM-generated explanations during the embedding process.

## C.2. LLM Querying and Output Length Control

In line with prior observations that large language models often generate overly verbose outputs (Nayab et al., 2025), we control the response length through meticulous prompt design to improve conciseness and computational efficiency. Specifically, we instruct the LLM to:

1. Limit its reasoning to at most three potential categories for classification tasks or three representative numerical values for regression tasks.
2. Restrict the total answer length within a budget of  $\mathcal{B}$  words.

In our implementation, we fix  $\mathcal{B} = 50$ .

## C.3. Prompts

To ensure the reproducibility and consistency of the explanation features, we employ a unified prompt structure across all datasets. The prompt consists of a task-specific question followed by a fixed set of reasoning and formatting constraints.

**Unified Prompt Structure** All prompts follow the template defined below. The placeholder [Task-specific Question] is replaced by the corresponding query for each dataset as listed in Table 9.

### General Prompt Template

**Question:** [Task-specific Question] If multiple [options/values] apply, provide a comma-separated list ordered from most to least related, then for each choice you gave, explain how it is present in the text. Please limit the number of output [categories/numerical values] to 3 and limit the answer length to 50 words.

**Answer:**

**Task-specific Questions** Table 9 enumerates the specific questions and constraints applied to each dataset.

Table 9. Task-specific components for the LLM prompt template.

Dataset	[Task-specific Question]	Constraint Type
<i>Amazon User LTV</i>	What is the total \$ value of purchases this customer node will make in the next 3 months?	Numerical Values
<i>Amazon Item LTV</i>	What is the total \$ value of purchases this product node will receive in the next 3 months?	Numerical Values
<i>Stack Post Votes</i>	What is the total number of votes this post node will receive in the next 3 months?	Numerical Values
<i>Instagram</i>	Which of the following categories does this user on Instagram belong to: Normal Users, Commercial Users?	Categories
<i>Computer</i>	Which of the following sub-categories of computer items does this item belong to: Computer Accessories & Peripherals, Tablet Accessories, Laptop Accessories, Computers & Tablets, Computer Components, Data Storage, Networking Products, Monitors, Servers, Tablet Replacement Parts?	Categories
<i>Photo</i>	Which of the following sub-categories of photo items does this item belong to: Video Surveillance, Accessories, Binoculars & Scopes, Video, Lighting & Studio, Bags & Cases, Tripods & Monopods, Flashes, Digital Cameras, Film Photography, Lenses, Underwater Photography?	Categories

**Algorithm 2** HyperGrad: Approximate Hypergradient Computation

---

```

1: Input: validation loss  $\mathcal{L}_V$ , training loss  $\mathcal{L}_T$ , learnable node importance scores  $\lambda$ , model parameters  $\mathbf{w}$ 
2: Output: hypergradient  $\frac{\partial \mathcal{L}_V}{\partial \lambda}$ 
3:  $v \leftarrow \frac{\partial \mathcal{L}_V}{\partial \mathbf{w}}$ 
4:  $p \leftarrow v$ 
5: for  $j = 0$  to  $i$  do
6:    $v \leftarrow v \times \left( I - \frac{\partial^2 \mathcal{L}_T}{\partial \mathbf{w} \partial \mathbf{w}^T} \right)$ 
7:    $p \leftarrow p + v$ 
8: end for
9: Compute hypergradient:  $\frac{\partial \mathcal{L}_V}{\partial \lambda} \leftarrow -p \times \frac{\partial^2 \mathcal{L}_T}{\partial \mathbf{w} \partial \lambda^T}$ 
10: return  $\frac{\partial \mathcal{L}_V}{\partial \lambda}$ 

```

---

**C.4. Pesudo codes**

Algorithm 2 shows the approximate hypergradient computation via Neumann series for efficient bilevel optimization. Algorithm 3 shows the Gumbel-Softmax Top- $K$  sampling process with the Straight-Through Estimator (STE) to ensure differentiability in sparse node selection.

## D. Analysis

### D.1. Time complexity Analysis

The time complexity of Algorithm 2 is primarily determined by the Neumann series approximation used to estimate the inverse Hessian. This procedure involves one initial gradient computation on the validation set, followed by  $i$  iterations of Hessian-vector products (HVPs), and a final projection step. Each HVP can be computed efficiently via automatic differentiation, with the same time complexity as a standard gradient backpropagation pass, denoted  $\mathcal{O}(C_{\text{GNN}})$ , without explicitly forming the Hessian matrix. As a result, the overall complexity of the Neumann approximation is linear in the number of approximation steps:

$$\mathcal{O}(i \cdot C_{\text{GNN}}).$$

The overall time complexity of Algorithm 1 is governed by the nested bilevel optimization structure combined with the cost of Graph Neural Network (GNN) propagations. Let  $T$  and  $I$  denote the number of outer and inner iterations,

---

**Algorithm 3** GumbelTopK: Gumbel-Softmax Top- $K$  Sampling with Straight-Through Estimator

**Input:** learnable node importance scores  $\lambda = \{\lambda_1, \dots, \lambda_N\}$ , temperature  $\tau$ , sparsity  $K$ 
**Output:** differentiable mask  $\mathbf{m} \in [0, 1]^N$ 

- 1:  $\triangleright$  Perturbation and Relaxation
- 2:  $\mathbf{g} \leftarrow [g_i \sim \text{Gumbel}(0, 1) \text{ for } g_i \text{ in } \{1, \dots, N\}]$
- 3:  $\mathbf{z} \leftarrow (\lambda + \mathbf{g})/\tau$
- 4:  $\mathbf{p} \leftarrow \text{Softmax}(\mathbf{z})$
- 5:  $\triangleright$  Discretization via Top- $K$
- 6:  $\mathcal{S} \leftarrow \arg\text{-top- } K(\{p_i\}_{i=1}^N)$
- 7:  $h_i \leftarrow \mathbb{1}[i \in \mathcal{S}] \text{ for all } i \in \{1, \dots, N\}$
- 8:  $\triangleright$  Gradient Estimation
- 9: **return**  $\mathbf{m} \leftarrow K \cdot \mathbf{p} + \text{stop\_gradient}(\mathbf{h} - K \cdot \mathbf{p})$

---

respectively, and let  $C_{\text{GNN}}$  represent the computational cost of a single GNN forward-backward pass, which typically scales as  $\mathcal{O}(|\mathcal{E}|D + |\mathcal{V}|D^2)$ , for a graph with  $|\mathcal{V}|$  nodes,  $|\mathcal{E}|$  edges, and node embedding dimension  $D$ . In each outer iteration, the algorithm performs  $I$  model update steps and one hypergradient computation involving  $i$  Neumann approximation steps. Hence, the total time complexity is

$$\mathcal{O}(T \cdot (I + i) \cdot C_{\text{GNN}}).$$

Additionally, we incorporate the computational cost of the Sparse Querying component. During each outer iteration, Sparse Querying selectively generates explanation texts and re-encodes features only for a sparse subset of nodes  $\mathcal{V}_{\text{expl}}$  with cardinality  $K$ . The per-iteration cost for this step is

$$\mathcal{O}(K \cdot (C_{\text{LLM}} + C_{\text{LM}})),$$

where  $C_{\text{LLM}}$  and  $C_{\text{LM}}$  indicate the computational cost of a single LLM inference and LM encoding, respectively.

Note that the full initial encoding of all node texts using the fixed LM, which requires  $\mathcal{O}(|\mathcal{V}| \cdot C_{\text{LM}})$  time, is performed once prior to the bilevel optimization and is thus excluded from the iterative complexity.

Consequently, the overall time complexity of Algorithm 1 including Sparse Querying is

$$\mathcal{O}(T \cdot (K \cdot (C_{\text{LLM}} + C_{\text{LM}}) + (I + i) \cdot C_{\text{GNN}})).$$

Because  $K \ll |\mathcal{V}|$  and both LLM and LM are frozen models performing forward-only passes, the Sparse Querying overhead remains well controlled. This design ensures efficient and scalable training of the graph LLM model on large text-attributed graphs.

Since  $C_{\text{LLM}}$  is significantly larger than both  $C_{\text{LM}}$  and  $C_{\text{GNN}}$ , and the number of outer iterations  $T$  is fixed and relatively small (set to 3 in our experiments), the overall time complexity of the algorithm 1 is dominated by the Sparse Querying's LLM inference cost. Therefore, the asymptotic time complexity can be approximated as

$$\mathcal{O}(K \cdot C_{\text{LLM}}).$$

This highlights that, despite incorporating sophisticated bilevel optimization and GNN training steps, the computational bottleneck lies in the selective LLM calls for explanation generation on a sparse subset of nodes. Our adaptive sparse querying strategy, which keeps  $K$  substantially smaller than  $|\mathcal{V}|$ , thus plays a critical role in enabling the practical efficiency of the proposed framework.

## D.2. Analysis on Ablation Study of Sparse Selection Strategy

**Performance Analysis.** The results in Table 5 demonstrate that BOSQ consistently achieves the highest accuracy across both datasets, outperforming random, similarity-based, and uncertainty-based heuristics. Specifically, **Local Dissimilarity** targets potential outliers via static feature distributions, while **Prediction Entropy** selects nodes with high model uncertainty. However, as shown in Table 5, these heuristics often provide inconsistent gains; for instance, Prediction Entropy slightly

improves performance on Instagram but underperforms on Photo compared to Local Dissimilarity. In contrast, our bilevel approach *dynamically* identifies nodes that provide the maximum gradient-based utility within the GNN’s optimization landscape. By directly optimizing the selection mask for the validation loss, BOSQ transcends simple heuristic signals to capture the complex synergy between graph topology and LLM-derived features, leading to more robust performance gains across different graph domains.

**Complexity and Efficiency Analysis.** A common concern regarding bilevel optimization is the potential computational burden of calculating hypergradients. As shown in Table 5, the time overhead of our method remains highly competitive. On Instagram, BOSQ’s total time (129.04s) is even lower than Prediction Entropy (141.02s), which requires a full forward pass of the pre-trained model on all nodes to compute logits and entropy. On the larger Photo dataset, the additional overhead of bilevel optimization is more pronounced but still remains within a practical range. To understand this efficiency, we analyze the theoretical complexity. The iterative optimization of the selection mask only adds marginal cost relative to the GNN training. By employing the Neumann series approximation (Lorraine et al., 2020), the cost of computing the hypergradient is  $\mathcal{O}(i \cdot C_{\text{GNN}})$ , where  $i$  is the number of terms and  $C_{\text{GNN}}$  is the cost of a standard GNN pass. Critically, in the context of GraphLLMs, the total runtime is heavily dominated by the LLM inference phase ( $C_{\text{LLM}}$ ), where  $C_{\text{LLM}} \gg C_{\text{GNN}}$ . Thus, the slight increase in training time is a small, worthwhile investment that enables a massive reduction in the number of required LLM queries, confirming the scalability of BOSQ for large-scale TAGs.

### D.3. Analysis on Transferability of Importance Scores

We hypothesize that using a shallow proxy mitigates the risks of overfitting and over-smoothing that typically plague bilevel optimization on deep GNNs. Specifically, the 5-layer model’s large capacity may lead the selector to overfit the training set by selecting “shortcut” nodes that provide immediate but poorly-generalizable gains. In contrast, the 1-layer model acts as an implicit regularizer, forcing the selector to prioritize nodes whose local structural and textual signals are most informative. Furthermore, deeper GNNs often suffer from over-smoothing, which blurs node distinctiveness and results in fuzzy gradient signals that make it difficult for the selector to identify true “information sources.” By utilizing a 1-layer proxy, BOSQ preserves individualized node features and avoids the amplification of structural noise, thereby providing cleaner and more transferable importance scores that effectively complement the LLM’s knowledge across different GNN depths.

### D.4. Sensitivity Analysis for Selective Querying Budget $K$

To provide further insights into the trade-off between computational efficiency and predictive performance, we conduct a sensitivity analysis on the hyperparameter  $K$ , which represents the budget for selective LLM querying. We evaluate BOSQ on the Instagram dataset with  $K \in \{2, 5, 10, 20, 50\}$ . The results are summarized in Table 10.

Table 10. Sensitivity analysis of the query budget  $K$  on the Instagram dataset. The default setting used in our main experiments is  $K = 10$  (highlighted in gray).

Budget $K$	Time (s) $\downarrow$	Accuracy (%) $\uparrow$	Std. Dev.
2	116.94	65.63	0.39
5	122.70	65.99	0.40
10 (Default)	129.04	66.22	0.55
20	144.52	66.29	0.23
50	197.18	66.44	0.48

**Observation and Justification for Default  $K = 10$ .** As observed in Table 10, the performance of BOSQ is remarkably robust across a wide range of budgets. Specifically, even with an extremely restricted budget ( $K = 2$ ), BOSQ achieves 65.45% accuracy, demonstrating the effectiveness of our adaptive querying strategy in identifying the most critical nodes. As  $K$  increases from 2 to 10, we observe a steady gain in accuracy (+0.59%) with only a minor increase in computational time (10.3%). However, further increasing  $K$  beyond our default value (from 10 to 50) yields diminishing returns: the accuracy only marginally improves by 0.22%, while the computational overhead increases significantly by 52.8% (from 129.04s to 197.18s). This trend justifies our choice of  $K = 10$  as the default hyperparameter, as it serves as an optimal “sweet spot” that balances predictive power and computational efficiency. The stable standard deviation across different values of  $K$  further validates the reliability of our bilevel-optimized sparse querying.

## E. Limitations and Future Work

While BOSQ establishes a principled bilevel optimization framework for sparse graph querying, several avenues remain to generalize its applicability and expressivity. First, beyond the current generative explanation paradigm, future work may extend the selection mechanism to discriminative LLM-as-Encoder settings. Second, relaxing the static cardinality constraint in favor of dynamic budgeting or nucleus sampling (Top-P) would allow for finer-grained, graph-wise computational adaptivity. Finally, while the current learnable vector parameterization ensures efficiency, upgrading the selector to non-linear architectures, such as Multi-Layer Perceptrons (MLPs), could significantly bolster the model’s capacity to capture complex topological dependencies.